Draft version May 6, 2014
Preprint typeset using LaTeX style emulateapj v. 08/13/06

arXiv:1405.0687v1 [astro-ph.HE] 4 May 2014

AN X-RAY SPECTRAL MODEL FOR CLUMPY TORI IN ACTIVE GALACTIC NUCLEI

Yuan Liu (刘元) and Xiaobo Li (李小波)
Key Laboratory of Particle Astrophysics, Institute of High Energy Physics, Chinese Academy of Sciences, P.O.Box 918-3, Beijing 100049, China

Draft version May 6, 2014

ABSTRACT

We construct an X-ray spectral model for the clumpy torus in an active galactic nucleus (AGN) using Geant4, which includes the physical processes of the photoelectric effect, Compton scattering, Rayleigh scattering, γ conversion, fluorescence line, and Auger process. Since the electrons in the torus are expected to be bounded instead of free, the deviation of the scattering cross section from the Klein-Nishina cross section has also been included, which changes the X-ray spectra by up to 25% below 10 keV. We have investigated the effect of the clumpiness parameters on the reflection spectra and the strength of the fluorescent line Fe Kα. The volume filling factor of the clouds in the clumpy torus only slightly influences the reflection spectra, however, the total column density and the number of clouds along the line of sight significantly change the shapes and amplitudes of the reflection spectra. The effect of column density is similar to the case of a smooth torus, while a small number of clouds along the line of sight will smooth out the anisotropy of the reflection spectra and the fluorescent line Fe Kα. The smoothing effect is mild in the low column density case ($N_{\rm H} = 10^{23}$ cm^{-2}), whereas it is much more evident in the high column density case ($N_{\rm H} = 10^{25}$ cm^{-2}). Our model provides a quantitative tool for the spectral analysis of the clumpy torus. We suggest that the joint fits of the broad band spectral energy distributions of AGNs (from X-ray to infrared) should better constrain the structure of the torus.

Subject headings: galaxies: Seyfert — X-rays: galaxies — radiative transfer

1. INTRODUCTION

In the unified model of active galactic nuclei (AGNs), a dusty torus is proposed to account for the apparent difference between type 1 and 2 AGNs, i.e., the central source is obscured by the torus in type 2 AGNs but not in type 1 AGNs (Antonucci 1993; Urry & Padovani 1995). Despite the key ingredient of the unification model, the origin and structure of the torus are still not clear. An important debate about the torus structure is whether the material in a torus is smooth or clumpy (Feltre et al. 2012; Hönig 2013). Both models have their advantages and drawbacks. The torus absorbs high-energy photons from an accretion disk/corona and converts them into the infrared band. Therefore, it is possible to constrain the structure of a torus by its infrared spectrum. The smooth model predicts strong silicate features in the infrared band; however, the observed feature is much weaker than the model's prediction (Laor & Draine 1993; Nenkova et al. 2002; Nikutta et al. 2009). The clumpy model can naturally explain the weakness of the silicate feature but cannot produce sufficient near-infrared emission from hot dust (Mor et al. 2009; Vignali et al. 2011). For a few nearby sources, the near-infrared interferometers can directly constrain the structure of the tori and indeed favor the clumpy model (Tristram et al. 2007). However, this method is limited by the low sensitivity of the infrared interferometer and cannot be applied to a large sample. By fitting the infrared energy spectral distribution with a specific model (smooth or clumpy), we can also obtain the parameters of the particular model. It has recently been claimed that the covering factors of type 2 AGNs are systematically larger than those of type 1 AGNs (Elitzur 2012).

Besides the infrared emission, the torus will also absorb and reflect the X-ray photons. Therefore, the X-ray spectrum can provide independent constraints on the structure of a torus. There are many works on the reflection spectra of different geometries. The commonly used model `pexrav` in *XSPEC* accounts for the reflection from a flat disk with infinite optical depth (Magdziarz & Zdziarski 1995). However, fluorescence lines are not self-consistently included in this model. The Gaussian lines should be manually added in the fit model of real X-ray spectra. This work is then improved by including the fluorescence line (e.g., `pexmon`), the ionization state of the reflection disk, and relativistic effects around a black hole (Nandra et al. 2007; Ross & Fabian 2005; Brenneman & Reynolds 2006). For the smooth torus, detailed X-ray models are already available (Ikeda et al. 2009; Murphy & Yaqoob 2009; Brightman & Nandra 2011), though the results are slightly different due to the discrepancies in geometry, cross section, and simulation methods used. Some works have also discussed the X-ray spectrum for clumpy media but do not dedicate to tori (Nandra & George 1994; Tatum et al. 2013). Yaqoob (2012) discussed the qualitative effects on the reflection spectrum and Fe Kα line due to the clumpy structure.

It is necessary to utilize Monte Carlo simulations to deal with clumpy geometry. In this paper, we present detailed results of simulations on a clumpy torus. In Section 2, we will explain the simulation process and other assumptions about the clumpy torus. Then, the results of the reflection continuum and Fe Kα are presented in Sections 3 and 4, respectively. In Section 5, we summarize our results and discuss the implications for observations. As the first part of a series of papers, we

Electronic address: liuyuan@ihep.ac.cn; lixb@ihep.ac.cn

will only discuss the spectrum in this paper. The results of temporal response and polarization will be given in subsequent papers.

2. SIMULATION METHOD AND ASSUMPTIONS

We utilized an object-oriented toolkit, Geant4 (version 4.9.4),[1] to perform the simulations. Three classes are necessary to construct the simulation model in Geant4.

1 The geometry and material of the interaction region are described by the class derived from G4VUserDetectorConstruction.

2 The class derived from G4VUserPhysicsList is required to construct the particles and physical processes to be activated in the simulation.

3 The class derived from G4VUserPrimaryGeneratorAction will generate the primary events, including the type, energy, direction, and position of the initial particles.

After the three classes have been defined, Geant4 will treat the particles one by one and track the trajectories of primary particles and secondary particles step by step. These particles will participate in the physical processes activated in the simulation. To determine the position of the interaction point of a given physical process, Geant4 first calculates the mean free path λ as the function of energy

$$\lambda(E) = (\sum_i [n_i \cdot \sigma(Z_i, E)])^{-1}, \quad (1)$$

where n_i is the number density of the ith element, $\sigma(Z_i, E)$ is the cross section per atom of the process, and $\sum_i []$ means the sum of all elements of the torus. Then the number of the mean free paths the particle travels before the interaction point is randomly determined by $-\log(\eta)$, where η is uniformly distributed in the range (0, 1). If the particle is absorbed or escapes from the world boundary, the tracking of it will be ended.[2] The result of the relaxation of an exited atom is randomly determined by the atomic data adopted, e.g., fluorescent yields. The secondary particles (e.g., the Fe Kα photons) are also tracked according to the method above (Agostinelli et al. 2003).

At each step, Geant4 will record the information of particles, e.g., kinetic energy, momentum, position, time, and physical process involved. Then the recorded information of every step can be used to select the particles of interest. In the simulations in this paper, photons that escape from the world boundary are selected to construct the X-ray spectra in different situations. In the following sections, we will discuss the assumptions in the three classes of our simulations.

2.1. *Geometry and Constituents*

For comparison, we also performed simulations of a smooth torus. The geometry of the smooth torus is shown in Figure 1 (left). The boundaries are defined by the inner radius $R_{\rm in} = 0.1$ pc, the outer radius $R_{\rm out} = 2.0$ pc, and the half-opening angle $\sigma = 60°$. We assume that the gas is uniformly distributed in the torus. For the clumpy torus, we use the same parameters ($R_{\rm in}$, $R_{\rm out}$, and σ) to define the envelope of the torus, within which numerous spherical clouds are uniformly distributed. In addition, we need parameters to describe the clumpiness of the torus. There can be different choices of the free parameters. In our simulation, we use the volume filling factor ϕ, the number of clouds along the line of sight N, and total column density $N_{\rm H}$ as the input parameters. Other quantities, e.g., the radius of the cloud and the density of the gas in the cloud, can be derived from these input parameters. ϕ and N determine the total number and the size of clouds and $N_{\rm H}$ further determines the density of the gas in clouds. Figure 1 (right) is the configuration of the clumpy torus. In the following simulations, we fix the parameters of the envelope, since we focus on the comparison between the smooth and clumpy cases. It is easy to change the parameters of the envelope in the subsequent simulations if necessary. We further assume that the sizes of the clouds are the same and the density of the gas in the cloud is uniform. These assumptions are surely simplified compared with the realistic tori of AGNs. However, the assumption "uniform distribution" is widely used in the previous simulations about the smooth torus. Hence, we follow this assumption and mainly focus on how the clumpiness influences the spectra. More complex and realistic distributions will be investigated in future simulations. We have included elements with the abundances from Anders & Grevesse (1989). The gas in the cloud is assumed to be cold, i.e., all atoms are in their ground states.

2.2. *Physical Processes*

We invoked the low-energy electromagnetic process in Geant4, which is valid in the energy range from 0.25 keV to 100 GeV. For photons, we considered the photoelectric effect, Compton scattering, Rayleigh scattering, and γ conversion. Fluorescence and Auger processes were also loaded in the photoelectric effect. For electrons, ionization, bremsstrahlung, and multiple scattering were added in the process. The relevant cross sections and atomic data are adopted from EPDL97.[3] In spite of slightly different cross sections of the photoelectric effect used in previous simulations of torus, the most important difference is the cross section of scatterings in our simulations. Since the electrons in a torus are bounded, the Klein-Nishina cross section is not appropriate (Hubbell et al. 1975). For the scattering by bounded electrons, the cross section is divided into two parts, Rayleigh scattering (coherent scattering, i.e., the atom is still in the ground state after the scattering) and Compton scattering (incoherent scattering, i.e., the atom is excited after the scattering). The incoherent scattering dominates high-energy band and tends to the Klein-Nishina cross section as the energy increasing; while the coherent scattering is more important at low-energy band and its cross section is proportional to the square of the total number of the electrons in one atom.[4] As a result, both the total cross section and the angular distribution of scattered photons will deviate from the Klein-Nishina cross section. The importance of this correction further depends

[1] http://geant4.cern.ch/

[2] The world boundary defines the largest volume in Geant4 to contain all material. We define the world boundary in our simulations as a box centered at the origin O with side length 10^{20} cm.

[3] https://www-nds.iaea.org/epdl97/

[4] The relative importance of the coherent and incoherent scattering is graphically shown at http://shape.ing.unibo.it/html/graphics_of_form_factors.HTM.

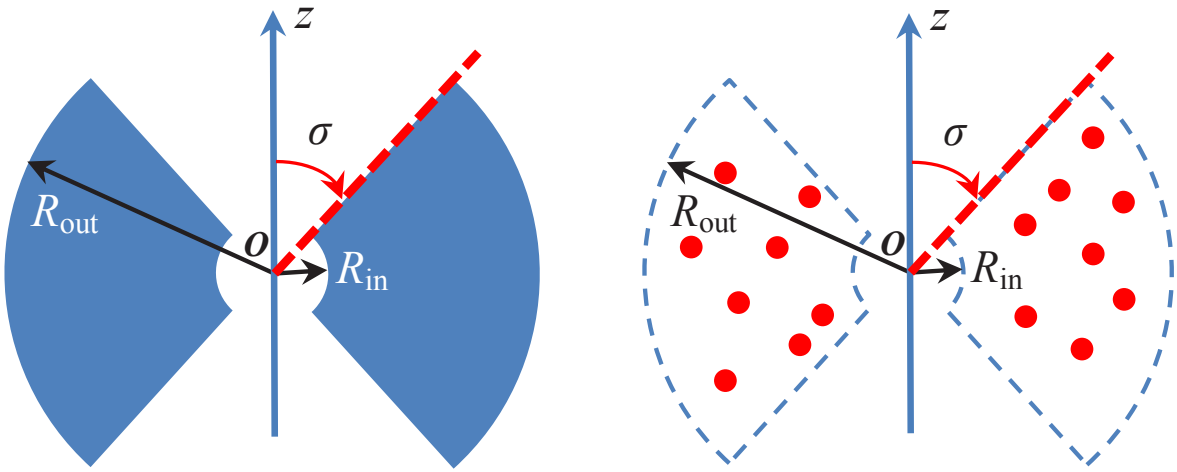

FIG. 1.— Cross-section view of the geometry of the smooth torus (left) and the clumpy torus (right) adopted in our simulations. For the smooth torus, the boundary is defined by the inner radius R_{in}, the outer radius R_{out}, and the half-opening angle σ; for the clumpy torus, the envelope of the clouds (red circles) is defined by the same parameters as for the smooth case. The central X-ray source is located at O.

on the abundance of the gas. To evaluate the amplitude of the deviation in the spectra, we replaced the cross section of scattering in Geant4 with the Klein-Nishina cross section and then compared the spectra with that using the default cross section in Geant4. An illustration of this comparison is shown in Figure 2. This correction is indeed more important for low-energy photons. The deviation is negligible above 10 keV and increases below 10 keV to 25% at 1 keV. Under the current abundance, helium is responsible for most of the deviation in the spectra. Therefore, this effect should be included in future simulations on the X-ray spectra of tori.

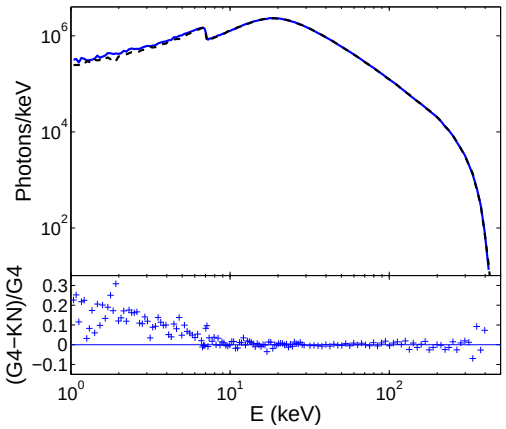

FIG. 2.— Comparison between spectra using the Klein-Nishina cross section (black dashed line) and the corrected cross section (blue solid line). The spectra are calculated with $N_H = 10^{25}$ cm^{-2}, $N = 2$, and $\phi = 0.01$ in the face-on direction (see the definition in Section 3).

2.3. *Incident Spectrum*

We adopted a single power law as the incident spectrum, i.e., flux $\propto E^{-\Gamma}$ (1 keV $\leq E \leq$ 500 keV), where Γ is the photon index and fixed at 1.8 throughout the simulations in this paper. The photons are isotropically emitted from the center O (see Figure 1), which is the location of the accretion disk/corona. The realistic X-ray spectrum of an AGN is usually more complex than a single power law and more components will induce curvature in the spectra. However, we intend to show the curvature produced by the torus itself and hence adopt this simple incident spectrum. It is convenient to include more complicated incident spectra in our simulation when we fit the observed spectrum.

3. REFLECTION SPECTRA

The N_H of the clumpy torus is actually the total column density if N clouds are exactly aligned along our line of sight. However, for a set of clouds, the number of clouds in different directions is nearly a Poisson distribution (Nenkova et al. 2008) with a mean of N and the portion of one particular cloud along the line of sight can be smaller than its diameter. As a result, the average column density is smaller than N_H. Figure 3 (left) shows the distribution of the number of clouds in some randomly selected directions for $N_H = 10^{24}$ cm^{-2}, $N = 10$, and $\phi = 0.01$ (the total number of clouds in the torus is about 1.4×10^7 under these parameters). The distribution of the cumulative column density (the sum of the column density of the intersected clouds in a particular direction) in different directions is shown in Figure 3 (right). The mean column density (or the equivalent N_H) is smaller than N_H by a factor of 0.66. If we reshape the spherical cloud into a cylinder with the same number density and with the axis pointing to the center, the height of the cylinder will be two-thirds of the diameter of the spherical cloud. This "geometry-average factor" is very close to the mean value in Figure 3 (right). Therefore, we compare the results of the clumpy torus with those of the smooth torus with $0.66N_H$. We should stress that this is not a unique method to calculate the "equivalent N_H" and there is actually no exact equivalence between a smooth torus and a clumpy torus. We intend to present a more meaningful comparison, but the clumpy torus is intrinsically different from the smooth case, which is actually the motivation of this paper.

For the smooth torus, the direct component (photons that escape from the torus without any interaction) of

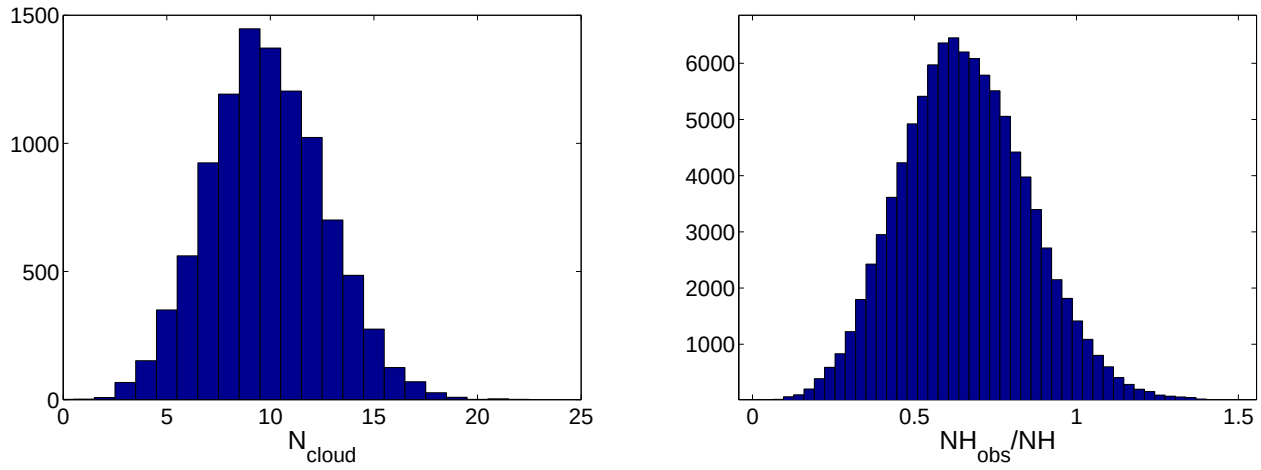

FIG. 3.— Statistics of the clouds for the case with $N_{\rm H} = 10^{24}$ cm^{-2}, $N = 10$, and $\phi = 0.01$. Left panel: the distribution of the number of clouds in different directions. Right panel: the distribution of the cumulative column density (normalized by $N_{\rm H}$) in different directions.

the transmitted spectrum is simply the incident spectrum weakened by the optical depth (determined by a single $N_{\rm H}$) due to photoelectric absorption and scattering along the line of sight. For the clumpy torus, if the size of the cloud is much larger than the compact corona of AGNs ($\lesssim$10 Schwarzschild radii), a single $N_{\rm H}$ for the direct component is still appropriate, which depends on the position of the cloud relative to the X-ray source (the corona). However, if our model is applied to a more extended X-ray source (i.e., the partial covering case), a geometry-averaged $N_{\rm H}$ should be applied to the direct component, which depends on the density distribution within the cloud and the brightness profile of the X-ray source. We will explore various possibilities in the comparison with the observed spectrum in future works. Then we will only discuss the reflection component, i.e., the scattered component, and the strength of the fluorescence line is presented in the next section.

In the following discussion, we divide the direction of the photons in the reflection spectra into 10 uniform bins according to $\cos\theta$ (θ is the angle between the direction of the photon and the z-axis in Figure 1). The bin $\cos\theta = 0 - 0.1$ and $\cos\theta = 0.9 - 1.0$ are defined as the edge-on and face-on directions, respectively. In Figure 4, we show the reflection spectra for different $N_{\rm H}$, N, ϕ, and $\cos\theta$. For clarity, only the spectra of edge-on and face-on cases are shown. The results of the smooth torus are also plotted for comparison. Next, we discuss the effect of the three clumpiness parameters ($N_{\rm H}$, ϕ, and N). The general effect of $N_{\rm H}$ is similar to the smooth case, e.g., the Compton hump and the anisotropy of the reflection spectra become more evident with increasing $N_{\rm H}$. The curvature above 200 keV is due to the decrease of the cross section of Compton scattering. Since the column density of one cloud is solely determined by N and $N_{\rm H}$, the filling factor ϕ only slightly impacts the spectra. However, the number of clouds along the line of sight significantly changes the column density of one cloud and further the shape of the spectra. As more low-energy photons can escape from the torus with a smaller N (the photons scattered by the clouds in the far side of the torus can leak from "holes" in the near side of the torus), the reflection spectra become more isotropic. We show the distribution of photons in the 5-6 keV band as a function of $\cos\theta$ in Figure 5, where the curves are normalized at the minima. With increasing $N_{\rm H}$, more photons in the edge-on direction are absorbed in the smooth case; however, the anisotropy of the reflection spectra is significantly weakened in the case of $N_{\rm H} = 10^{25}$ cm^{-2} and $N = 2$.

To better understand the effect of $N_{\rm H}$ and N on the reflection spectra, we show the single and multi-scattering spectra separately in Figure 6. A larger $N_{\rm H}$ is helpful to suppress the fraction of single scattering, i.e., the photons have a higher probability of scattering with the clouds before escaping from the torus. However, the spectrum of single scattering still dominates at the lower energies; the multi-scattering spectrum is more important at higher energies since it will experience more absorption during the scatterings. The multi-scattering spectrum is more evident for larger N, as there are more interfaces to produce scatterings. We show the histogram of the number of scatterings in Figure 7 for $N_{\rm H} = 10^{23}$ cm^{-2} and 10^{25} cm^{-2}. Both the maximum number of scatterings and the fraction of multi-scatterings increase with increasing $N_{\rm H}$. In addition, since the geometry covering factor of the clumpy torus is $(1 - e^{-N})\cos\sigma$ (Nenkova et al. 2008), the covering factor of $N = 2$ is smaller than that of $N = 10$ by a factor of 0.86.

4. THE STRENGTH OF FE Kα LINE

The fluorescent line Fe Kα is one of the most important lines in the X-ray band, which can reflect the structure and density of the torus. If the torus is optically thin to the photons of Fe Kα, the strength of Fe Kα can be simply calculated by a linear relation of the properties of the torus, e.g., column density, covering factor, and the abundance of iron (Krolik & Kallman 1987). Moreover, the Fe Kα photons are isotropically distributed. However, the optically thin approximation is not valid for Fe Kα photons if the column density of the torus is larger than 2×10^{22} cm^{-2} (Yaqoob et al. 2010). In this case, the geometry will impact the distribution of Fe Kα photons and numerical simulation is required to determine the luminosity of Fe Kα. We will investigate the relation between the anisotropy of Fe Kα and the parameters of clumpiness. In the following discussion, we have included the scattered Fe Kα photons (the so-

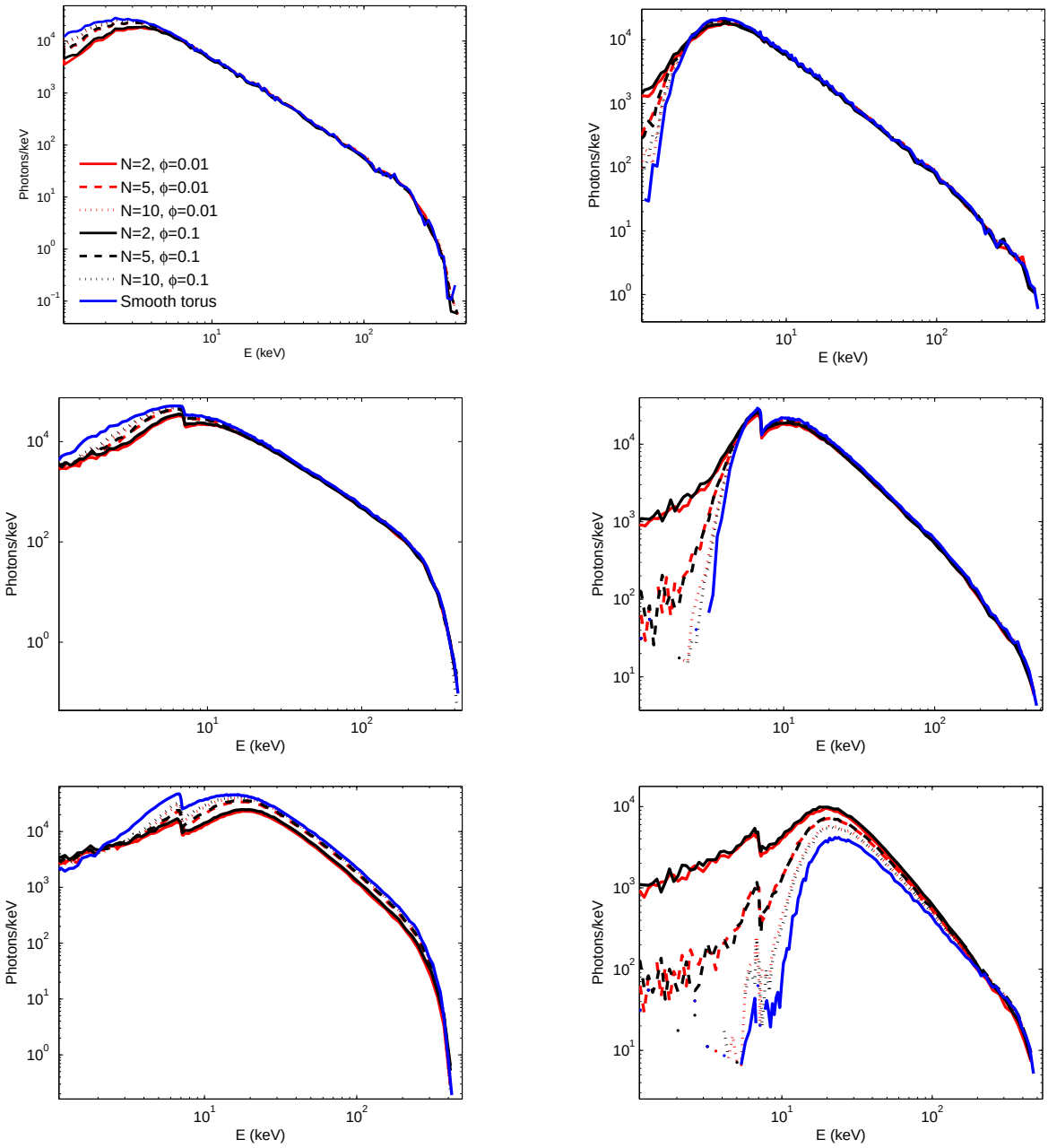

FIG. 4.— Reflection spectra. The top, middle, and bottom rows are for $N_{\rm H} = 10^{23}$ cm^{-2}, 10^{24} cm^{-2}, and 10^{25} cm^{-2}, respectively. Left column: $\cos\theta = 0.9 - 1.0$. Right column: $\cos\theta = 0 - 0.1$. In each panel, we show the reflection spectra of the smooth torus with the corresponding parameters for comparison. The meanings of curves are indicated in the legend of the first panel and the same for each panel.

called "Compton shoulder") into the total flux of Fe Kα. In Figure 8, we plot the distribution of Fe Kα photons as a function of $\cos\theta$, where the curves are normalized at the minima. Since the effect of ϕ is minor as shown in Figure 4, we will only discuss the results with different $N_{\rm H}$ and N but fix $\phi = 0.01$. The anisotropy increases with increasing $N_{\rm H}$, which is the simple result of more absorption in the edge-on direction in the high column density case. For the same equivalent $N_{\rm H}$, the anisotropy of Fe Kα in clumpy cases are weaker than the smooth case. More specifically, a smaller N will further suppress the anisotropy of Fe Kα. This effect is much more significant in the $N_{\rm H} = 25$ cm^{-2} case, which is similar to the situation of the reflection spectrum. Due to the limited statistics of the current simulations, we can only investigate the strength of Fe Kα. However, it is possible to extend our simulation and discuss other fluorescence lines.

5. SUMMARY AND DISCUSSION

To construct an X-ray spectral model for the clumpy torus in AGNs, we have performed simulations using an object-oriented toolkit Geant4, by which it is convenient to deal with complex geometry. Besides the necessary physical processes, e.g., photoelectric absorption, Compton scattering, and fluorescence lines, considered in previous simulations of tori, we have included corrections to the treatment of scattering by explicitly considering

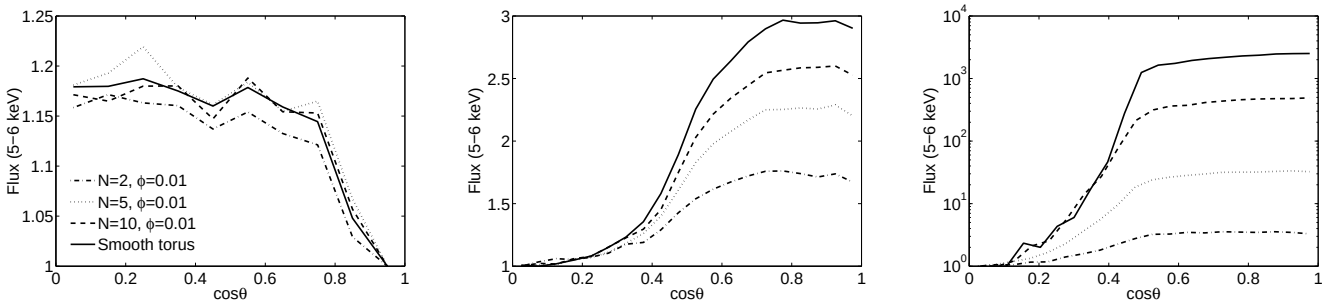

FIG. 5.— Distribution of the photons in reflection spectra (5-6 keV) as a function of $\cos\theta$ for $N_{\rm H} = 10^{23}$ cm^{-2} (left), $N_{\rm H} = 10^{24}$ cm^{-2} (middle), and $N_{\rm H} = 10^{25}$ cm^{-2} (right, logarithmic scale). The meanings of curves are indicated in the legend of the first panel and the same for each panel.

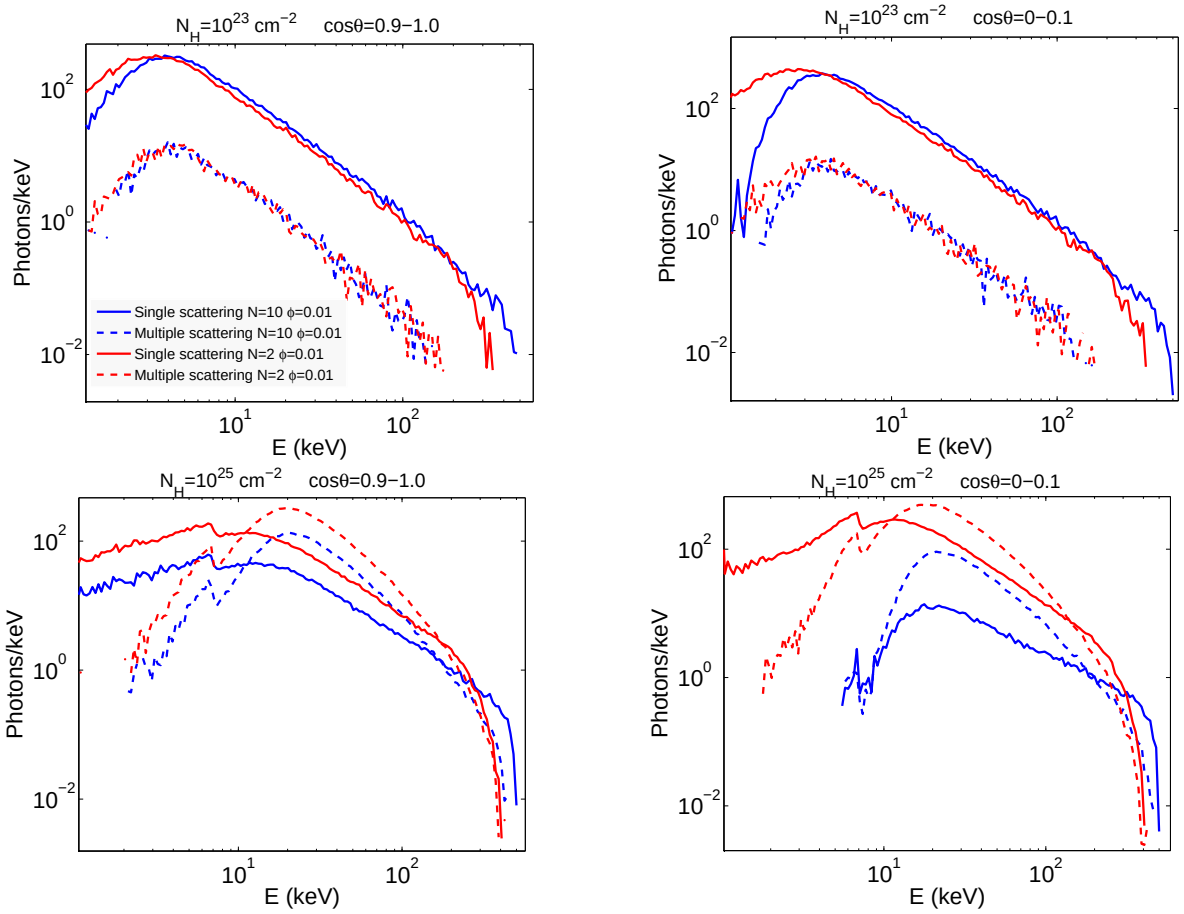

FIG. 6.— Single and multiple scattering spectra. The values of column density and $\cos\theta$ are shown in the title of each panel. The meanings of the curves are the same for each panel and labeled in the first panel.

Rayleigh (coherent) and Compton (incoherent) scattering from bound, rather than free, electrons. This correction can induce a deviation on the X-ray spectra up to 25% at 1 keV, therefore we cannot ignore it in the simulation of neutral tori. There are indications from the widths of the Fe Kα lines (Shu et al. 2010, 2011) that the location of the line-emitting material may be closer to the central engine than the traditional torus in some AGNs. Hence, the observed effects of the corrections may vary from AGN to AGN.

Different combinations of $N_{\rm H}$, ϕ, and N have been investigated. The filling factor only slightly changes the reflection spectra, while the number of clouds along the line of sight significantly influences the spectra. If there are more clouds, i.e., $N = 10$, the result is similar to the smooth case; while for the extreme case ($N_{\rm H} = 10^{25}$ cm^{-2} and $N = 2$), the shapes of the reflection spectra in different directions are quite similar expect for the somewhat lower amplitude in the edge-on direction, i.e., the reflection spectra become more isotropic. Therefore, if strong reflection components are found in the observed spectra of type 2 AGNs, the "clumpy" scenario could be invoked to explain the spectra. In this case, the quantitative spectral model presented in this paper is necessary

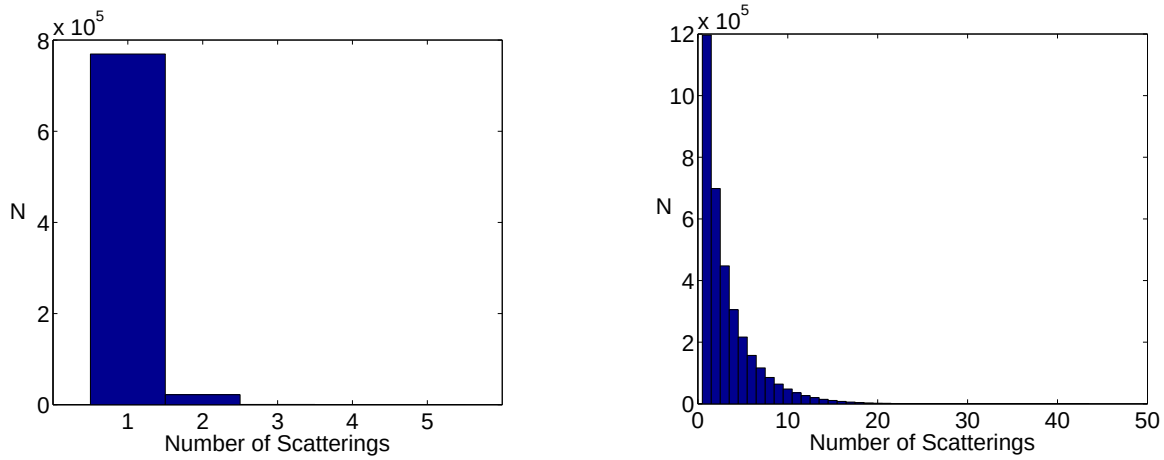

FIG. 7.— Histograms of the number of scatterings for $N_{\rm H} = 10^{23}$ cm^{-2}, $N = 10$, and $\phi = 0.01$ (left) and $N_{\rm H} = 10^{25}$ cm^{-2}, $N = 10$, and $\phi = 0.01$ (right).

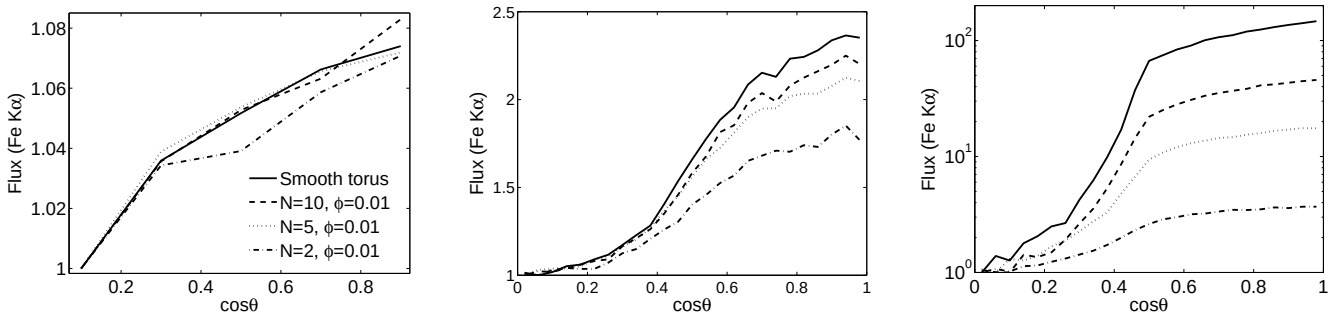

FIG. 8.— Distribution of the Fe Kα photons as a function of $\cos\theta$ for $N_{\rm H} = 10^{23}$ cm^{-2} (left), $N_{\rm H} = 10^{24}$ cm^{-2} (middle), and $N_{\rm H} = 10^{25}$ cm^{-2} (right, logarithmic scale). The meanings of the curves are labeled in the first panel and the same for each panel.

for the measurement of the structure of the clumpy torus.

Besides the reflection continuum, the anisotropy of the Fe Kα line will also be impacted by clumpiness. The situation is quite similar to the reflection continuum. In the low column density case ($N_{\rm H} = 10^{23}$ cm^{-2}), the distribution of Fe Kα photons is nearly isotropic and only slightly changed by the parameters of clumpiness, while for the high column density case ($N_{\rm H} = 10^{25}$ cm^{-2}), a smaller N significantly degrades the anisotropy of Fe Kα photons. The strength of Fe Kα has already been investigated in previous simulations of smooth tori and found to be anisotropic (though the result is expressed in the equivalent width of Fe Kα). The clumpy torus can further smooth out the anisotropy of the Fe Kα, which depends on the column density of the clouds. This result is similar to the explanation of the weakness of the silicate feature in the infrared spectra of AGNs (Nenkova et al. 2002).

In the observational aspect, since the X-ray continua of AGNs can be contaminated by other components not related to the torus, the luminosity of the Fe Kα line will provide independent evidence of the structure of the torus. For example, if there is no significant difference between the luminosities of Fe Kα lines in type 1 and 2 ($N_{\rm H} > 10^{23}$ cm^{-2}) AGNs, the "clumpy" torus is required according to the curves in Figure 8 or we should modify the unified model of AGNs as claimed by Elitzur (2012). The current observations have already provided some clues but are not conclusive. Liu & Wang (2010) found that the luminosities of the narrow Fe Kα lines in Compton-thin and Compton-thick type 2 AGNs are weaker than those in type 1 AGNs by a factor of 2.9 and 5.6, respectively. This difference is broadly consistent with the results for a smooth torus. However, from a smaller sample from *Chandra HETG*, Shu et al. (2011) found the Fe Kα line flux of type 2 AGNs is only marginally lower than that of type 2 AGNs, which will require the smoothing effect of a clumpy torus since the observed column density of Compton-thick AGN is already larger than 10^{24} cm^{-2}. A more complete sample of the luminosity of Fe Kα should be helpful in determining the geometry of a torus and the curves presented in Figure 8 will further constrain the parameters.

In principle, it is possible to combine the infrared spectral energy distribution and X-ray spectra to better constrain the structure of tori. However, it should be cautioned that the gas in a torus is only sensitive to X-ray photons but the dust can also absorb optical photons. Therefore, if the dust-to-gas ratio is not uniform in a torus (which is likely to be the case due to the temperature gradient in the torus), the structure of the torus probed by the X-ray photons can be different from that obtained from the infrared spectral energy distribution. We only present the X-ray spectral model for clumpy tori here, and the details of the comparison between the structure from X-ray and infrared bands will be presented in future works. The results from temporal and polarization observations should be further helpful to break the degeneracy of the clumpiness parameters of the torus (Hönig & Kishimoto 2010; Ramos Almeida et

al. 2011).

The authors thank the referee for useful comments which clarified the paper. This work is supported by 973 Program of China under grant 2009CB824800, and by the National Natural Science Foundation of China under grant Nos. 11103019, 11133002, and 11103022.

REFERENCES

Agostinelli, S., et al. 2003, Nucl. Instr. Meth., A506, 250
Anders, E., & Grevesse, N. 1989, Geochim. Cosmochim. Acta, 53, 197
Antonucci, R. R. 1993, ARA&A, 31, 473
Brenneman, L. W., & Reynolds, C. S. 2006, ApJ, 652, 1028
Brightman, M., & Nandra, K. 2011, MNRAS, 413, 1206
Elitzur, M. 2012, ApJL, 747, L33
Feltre, A., Hatziminaoglou, E., Fritz, J., & Franceschini, A. 2012, MNRAS, 426, 120
Hönig, S. F. arXiv:1301.1349
Hönig, S. F., & Kishimoto, M. 2010, A&A, 523, A27
Hubbell, J. H., et al. 1975, Journal of Physical and Chemical Reference Data, 4, 471
Ikeda, S., Awaki, H., & Terashima, Y. 2009, ApJ, 692, 60
Krolik, J. H., & Kallman, T. R. 1987, ApJL, 320, L5
Laor, A., & Draine, B. T. 1993, ApJ, 402, 441
Liu, T., & Wang, J. X. 2010, ApJ, 725, 2381
Magdziarz, P., & Zdziarski, A. A., 1995, MNRAS, 273, 837
Mor, R., Netzer, H.,& Elitzur, M. 2009, ApJ, 705, 298
Murphy, K. D., & Yaqoob, T. 2009, MNRAS, 397, 1549
Nandra, K., & George, I. M. 1994, MNRAS, 267, 974
Nandra, K., O'Neill, P. M., George, I. M., & Reeves, J. N. 2007, MNRAS, 382, 194
Nenkova, M., Ivezić, Ž., & Elitzur, M. 2002, ApJL, 570, L9
Nenkova, M., Sirocky, M. M., Ivezić, Ž., & Elitzur, M. 2008, ApJ, 685, 147
Nikutta, R., Elitzur, M., & Lacy, M. 2009, ApJ, 707, 1550
Ramos Almeida, C., Levenson, N. A., Alonso-Herrero, A., et al. 2011, ApJ, 731, 92
Ross, R. R., & Fabian, A. C. 2005, MNRAS, 358, 211
Shu, X. W., Yaqoob, T., & Wang, J. X. 2010, ApJS, 187, 581
Shu, X. W., Yaqoob, T., & Wang, J. X. 2011, ApJ, 738, 147
Tatum, M. M., Turner, T. J., Miller, L., & Reeves, J. N. 2013, ApJ, 762, 80
Tristram, K. R. W., Meisenheimer, K., Jaffe, W., et al. 2007, A&A, 474, 837
Urry C. M., & Padovani P., 1995, PASP, 107, 803
Vignali, C., Piconcelli, E., Lanzuisi, G., et al. 2011, MNRAS, 416, 2068
Yaqoob, T. 2012, MNRAS, 423, 3360
Yaqoob, T., Murphy, K. D., Miller, L., & Turner, T. J. 2010, MNRAS, 401, 411 12